Failure mechanism and treatment measures of supporting structures at portal for a shallow buried and asymmetrically loaded tunnel with small clear-distance

Hao Chen
Shaoxing University
Hongpeng Lai (laihp168@chd.edu.cn)
Chang'an University School of Highway
Man Huang
Shaoxing University
Gang Wang
Shaoxing University
Qiang Tang
Soochow University

Research Article

Keywords: Tunnel engineering, Shallow buried and asymmetrically loaded, Small clear-distance, Failure mechanism, Treatment measures.

Posted Date: June 8th, 2022

DOI: https://doi.org/10.21203/rs.3.rs-1621353/v1

Abstract

The construction of tunnel portal not only has to face the challenges of complex geological conditions such as shallow buried and asymmetrically loaded, but also needs to consider the adverse effects of factors such as the layout form of the tunnel. Thus, the construction of portal has always been the difficulty and focus of tunnel engineering construction. Under the coupling of multiple adverse factors such as complex geological conditions and special layout form, the tunnel portal is prone to excessive deformation, supporting structures cracking and even collapse during the excavation. In this study, a shallow buried and asymmetrically loaded tunnel with small clear-distance in northwest China was taken as an engineering case. Aiming at the distresses of slope instability, peeling off and block falling of primary support concrete and cracking of secondary lining concrete in the tunnel portal construction, combined with field investigation, statistical analysis, numerical simulation and deformation monitoring, the failure mechanism of supporting structures was deeply studied, and the corresponding treatment measures were proposed. The research results indicated that the loose and broken gravel soil in the shallow buried section, asymmetrical loading, surface water infiltration, and short construction spacing between two tunnels were the main triggers of supporting structures failure. Affected by the topographic bias, the loose load generated by the surrounding rock on the deep buried side squeezed the entire tunnel to the shallow buried side after the portal excavation. And this deformation trend became more significant after the gravel soil was deteriorated by water immersion. The retaining wall produced a clockwise rotation deformation around the wall corner in the process of limiting the tunnel deviation, and the local wall body cracked due to the excessive tensile stress. The primary support concrete and secondary lining concrete produced excessive asymmetrical deformation because of the significant asymmetrical loading. The concrete with excessive deformation was cracked by obvious tensile or shear stress. The following tunnel excavation had a significant negative impact on the stability of the prior tunnel. Combining the failure mechanism of the supporting structures and the characteristics of the continuous development of cracks, the treatment measures of ‘stabilize the stratum first and then treat the cracks’ were proposed, including the backfilling and tamping the shallow buried side at tunnel portal, reinforcing the interlaid rock by ground surface grouting, setting intercepting ditch at the slope top, staggering a certain safe excavation distance between the following tunnel and the prior tunnel. The field monitoring and patrol inspection results indicated that the proposed treatment measures had achieved the expected results. The research results can provide corresponding construction experience and suggestions for similar projects in the future.

1 Introduction

In recent years, with the gradual expansion of transportation infrastructure construction in China, a large amount of tunnels and underground projects have been put into construction. Despite the remarkable development of tunnel construction technologies, the problem of difficult in excavating tunnel portal is still widespread in the process of entire tunnel engineering construction. As the throat part of the tunnel project, the portal section has always been the difficulty and focus of construction. The tunnel portal is

often located in the stratum with severe weathering of surrounding rock and complex terrain. These factors will have a serious negative impact on the safe construction of the tunnel portal. If the excavation methods, supporting and auxiliary measures were unreasonable during the tunnel portal construction, it would be extremely easy to cause distresses such as excessive deformation of surrounding rock, cracking and failure of supporting structures, and even collapse. These distresses not only cause construction delay and property loss, but also seriously threaten the personal safety of construction personnel.

Shallow buried and asymmetrical terrain is the most common adverse geological conditions encountered during the tunnel portal excavation. Compared with the general type of tunnel, the shallow and asymmetrically loaded tunnel often exhibits significant asymmetric settlement and local stress concentration during the excavation process, and it is more prone to occur failure of the supporting structures (Qiu et al. 2015; Yang et al. 2020). The current researches on shallow and asymmetrically loaded tunnel mainly focus on the following aspects, namely the calculation of tunnel overlying surrounding rock pressure (Qiu et al. 2015; Zuo et al. 2011; Bai and Wu 2012; Yang et al. 2013b), the study of deformation and stress characteristics of tunnel structure (Lei et al. 2015; Liu et al. 2017; Yang and Wang. 2008; Pan et al. 2011), the optimization of excavation methods and supporting measures (Xiao et al. 2016; Yang et al. 2013a), and the reveal of supporting structures failure mechanism (Yang et al. 2020; Zhang et al. 2017; Xiao et al. 2014). Combined with laboratory model test and limit analysis method, Qiu et al. (2015) constructed the failure model of tunnel with shallow buried and asymmetrical loading, and deduced the upper bound solution of the tunnel overlying surrounding rock pressure based on the principle of virtual power. Zuo (2011) and Bai et al. (2012) pointed out that the overlying surrounding rock pressure calculation of shallow and asymmetrically loaded tunnel recommended in ‘Code for design of road tunnel in China’ (JTG 3370.1–2018) had limitations. Therefore, the calculation formula was modified by constructing a new calculation model or programming method, and the modified formula was verified with the simulated results and measured data in actual engineering. Based on similarity theory and elastic mechanics equations, Lei et al. (2015) analyzed the stress distribution laws and failure mechanism of the surrounding rock and lining concrete under different degree of asymmetrical loading by designing various groups model tests. By centrifugal test and finite element simulation method, Liu et al. (2017) compared and analyzed the failure modes and stress distribution laws of the surrounding rock at shallow and asymmetrically loaded tunnel portal in bedding stratum and homogeneous stratum. Relying on a shallow and asymmetrically loaded tunnel crossing a large loose sediment layer, Xiao et al. (2016) compared the stability of tunnel structure when excavated by upper and lower bench method, the three-bench method, and the single side drift method. The single side drift method was recommended because of the significant advantages in controlling surrounding rock settlement, ameliorating lining stress and reducing disturbance zone area. Yang et al. (2013a) simulated the excavation process of an asymmetrically loaded tunnel under multi-factor coupling, and proposed that pre-reinforcement was required if the overlying surrounding rock was less than 15 m. Yang et al. (2020) analyzed the causing mechanism of the distresses during a shallow and asymmetrically loaded tunnel portal construction, it was found that the asymmetrical loading, the precipitation and the

inadequate construction management were the main reasons of failure event. With the finite element simulation, Zhang et al. (2017) investigated the cracking causes of secondary lining concrete at vault of multiarch tunnel. The results indicated that the shallow buried and bias on topography and the use of plain concrete led to the concrete cracking due to excessive tensile stress and negative bending moment.

In addition to objective factors such as topography and geological conditions, the subjective factors such as tunnel layout form, cross-section type, and cross-section area are also important considerations for what construction methods and support measures adopted in the tunnel portal. In the layout form of tunnel, compared with the separated tunnel, the small clear-distance tunnel has the advantages of less connection difficulty and small floor area; compared with the multiarch tunnel, it has the advantages of giving full play to self-supporting ability of interlaid rock, short construction period, and easy control of construction quality. Therefore, the small clear-distance tunnel has been widely used in specific terrain and geological conditions. Domestic and foreign scholars have conducted in-depth researches on the construction mechanics characteristics of the small clear-distance tunnel. Based on multiple small clear-distance tunnels in Japan, Kawada et al. (1996) carried out a systematic study on the design, construction and blasting control technology of this type of tunnel. By model tests and field monitoring methods, Kim (2004), Wen (2004) and Lee et al. (2006) pointed out that the mutual influence of the construction of the prior tunnel and following tunnel would become obvious when the clear distance of the small clear-distance tunnel was less than one time of the tunnel width. Combined with the limit analysis method and reliability theory, Zhang et al. (2018) introduced the nonlinear failure criterion, and obtained the safe factors and corresponding critical clearance of twin shallow tunnel under different safety levels. With field monitoring and numerical simulation methods, Xia (2007), Jiang (2012), Cui (2019) and Jiang et al. (2019) studied the deformation mechanism, construction mechanical behavior and structural stability of large cross-section and small clear-distance tunnels. It was found that the following tunnel excavation obviously affected the prior tunnel stability, and the special excavation methods (such as CD, CRD and double sides drift method) and auxiliary measures (such as pre-reinforcement and interlaid rock reinforcement) must be carried out to alleviate the negative impact. The reinforcement measure of isolation piles was put forward by Lv et al. (2020) in Guangzhou Metro Line 8, to mitigate the mutual influence of two shield tunnel construction with small clear distance. Jiao et al. (2019) used finite element method to study the deformation characteristics of double-line shield tunnel construction under different clear distances, and considered that if the distance between two tunnels was less than 0.8 times the tunnel diameter, the corresponding reinforcement measures should be taken to ensure the surrounding rock stability.

At present, the researches on shallow buried and asymmetrically loaded tunnels and small clear-distance tunnels have been more in-depth, and rich design and construction experience has been accumulated. However, the research on tunnel engineering design and construction under the coupling of multiple adverse factors, such as loose and broken surrounding rock, shallow buried and asymmetrical terrain, and layout form of small clear-distance, was still relatively rare. It is stipulated in the ‘Code for design of road tunnel in China’ that if there is a small clear-distance tunnel with asymmetrical loading, the support parameters, construction methods and excavation sequence need to be specially designed (JTG 3370.1–

2018). However, in actual projects, the design and construction of shallow and asymmetrically loaded tunnels with small clear-distance mostly rely on engineering experience. And the topographical and geological conditions encountered in the tunnel portal are changeable and different. During the construction of this type of tunnel portal, the engineering accidents continue to emerge, and the failure mechanism has not yet been explored in detail. Therefore, it is very necessary to conduct in-depth research on the distresses causing mechanism in the construction of shallow and asymmetrically loaded tunnel portal with small clear-distance, which can timely propose targeted treatment and prevention measures and reduce the possibility of various distresses. The research results can also provide basis and experience for similar tunnel engineering design and construction in future.

In this study, a shallow buried and asymmetrically loaded tunnel with small clear-distance in northwest China was taken as an engineering case. The field investigation and statistics of the failure of supporting structures during tunnel portal construction were carried out first. Combined with three-dimensional numerical simulation and field monitoring method, an in-depth study for the failure mechanism of the supporting structures were conducted. And then the corresponding treatment measures were proposed based on the research results, which were successfully applied to the actual project finally.

2 Project Overview

2.1 Topographic and geomorphic characterization

The studied tunnel is located in northwest China, and it is a separated bidirectional four-lane highway short tunnel. The starting and ending chainage of the left tunnel is ZK39 + 843-ZK40 + 177, with a length of 334 m; the right tunnel is YK39 + 866-YK40 + 166, with a length of 300 m. The net height and width of tunnel is 8.98 m and 10.86 mm respectively, and the maximum buried depth is about 60 m. The minimum distance between the left and right tunnel axis is only 13.2 m at the portal section, which belongs to a typical small clear-distance tunnel, as shown in Fig. 1.

The overlying stratum of the tunnel is mainly light-gray Quaternary Deluvial gravelly soil (Q_4^{dl}), which is composed of gravel, block stone and humus silt, with dense surface plant roots and developed wormholes, as shown in Fig. 2. The overall structure of this stratum is loose and the stability is poor. The average layer thickness is about 17.4 m. The underlying stratum is mainly yellow-brown Lower Triassic sandy slate intercalated with sandstone (T_1), with dense and hard rock and good stability.

The tunnel portal is located in the gravel soil layer. The overburden thickness of right tunnel portal is less than 3.0 m and the slope gradient exceeds 30°, which belongs to a typical shallow buried and asymmetrically loaded tunnel portal, as shown in Fig. 3. According to the results of field drilling exploration and laboratory rock mechanics tests, the surrounding rock grade from the portal section to YK/ZK39 + 930 is classified as grade Ⅴ.

Groundwater in the tunnel site area is relatively scarce. It is mainly composed of bedrock fissure water and Quaternary pore phreatic water, which is supplied by atmospheric precipitation and stored in the gravel soil layer. The surface water is abundant. Multiple streams are developed on the surface, which eventually flow into a large river nearby. Moreover, in rainy season, the precipitation is abundant and heavy rainstorms often occur.

2.2 Construction method and supporting measures at portal

The tunnel was constructed by new Austrian method, and the upper and lower bench method was adopted for excavation. Due to the serious shallow and asymmetrical loading in the portal, the right tunnel near the shallow buried side was excavated first, and then the left tunnel near the deep buried side was excavated, keeping a certain distance between two tunnel faces. The composite lining was supported for tunnel supporting. The primary support measures included 3.5 m long R25 hollow grouting anchor bolts, with a longitudinal spacing of 75 cm and a circumferential spacing of 100 cm; φ6 double-layer steel mesh, setting with 20×20 cm spacing; I20a I-steel with a spacing of 75 cm; C25 shotcrete with a thickness of 26 cm. The secondary lining adopted C30 reinforced concrete with a thickness of 50 cm. To ensure safe excavation of the portal, the 40 m long φ108×6 mm large pipe shed was construct before the excavation, with a circumferential spacing of 40 cm. For the severe topographic bias, the 10 m long C25 concrete retaining wall was designed on the right side of the tunnel portal. In the process of excavation, auxiliary measures such as pre-grouting pipe reinforcement and grouting reinforcement with lengthened anchor in interlaid rock were also adopted. The 3.0 m long φ42×4 mm hot-rolled seamless steel pipes were used in the pre-grouting pipe, with 15° extrapolation angle and 40 cm circumferential spacing. The 5.0 m long R25 hollow grouting anchor bolts were used to reinforce the interlaid rock, which were arranged at a distance of 75 cm in the longitudinal direction and 100 cm in the circumferential direction. The supporting measures at right tunnel portal were shown in Fig. 4.

3 Failure Of Supporting Structures At Portal

3.1 Failure of the slope and retaining wall

When the right tunnel was excavated to 8 m, the construction of the retaining wall had been partially completed, and the left tunnel portal began to excavate. When the left tunnel was excavated to 2 m, two obvious transverse cracks appeared at the slope above the right tunnel portal. The two cracks continued to develop and then extended to the ground surface during the construction, as shown in Fig. 5. And a large number of messy microcracks also appeared at the slope above the left tunnel portal. At the same time, the wall body of the retaining wall cracked at about 1.6 m and 5.3 m away from the ground (Fig. 5), and the crack width expanded gradually with the progress of construction. However, the cracking of the slope and the retaining wall did not cause the construction unit to pay enough attention. After re-brushing the slope and repairing the retaining wall cracks, the construction of the tunnel portal continued.

3.2 Cracking and block falling of the primary support concrete

The primary support concrete cracks first appeared at right tunnel portal, and mainly concentrated on the left arch shoulder and waist. When the right tunnel was excavated to YK39 + 902-YK39 + 910, more serious cracks appeared in the primary support concrete, which were mainly distributed at the vault, arch shoulder and arch waist. There was even a large area of concrete falling off at right side of the vault at YK39 + 902, as shown in Fig. 6. Meanwhile, a large number of small cracks with a width of 0.3 ~ 5 mm appeared in the primary support concrete of ZK39 + 870-ZK39 + 890 in the left tunnel, of which the circumferential cracks were the majority.

3.3 Cracking of the invert

Soon after the primary support concrete cracked, the construction workers found cracks in the invert filling layer at YK39 + 866-YK39 + 886.5 at right tunnel and ZK39 + 849-ZK39 + 857 at left tunnel while cleaning the sediment on the ground. The crack of right tunnel invert was about 20.5 m long and extended along the tunnel longitudinal direction. The location of the crack was about 1.3 m near the right side wall, with the width of about 3–10 mm. Many microcracks appeared on the right side of tunnel axis, and the number gradually increased with the excavation (Fig. 7a). The crack of left tunnel invert was about 8.0 m long and extended along the tunnel longitudinal direction, with the width of about 1–6 mm (Fig. 7b).

3.4 Cracking of the secondary lining concrete

The cracking of the secondary lining concrete at tunnel portal was also serious. The cracking locations were mainly concentrated in YK39 + 866-YK39 + 910 of right tunnel and ZK39 + 848-ZK39 + 877 of left tunnel. And the lining concrete cracking in right tunnel was significant more severe than that in left tunnel. The lining concrete at right tunnel portal cracked since the completion of pouring, and the scale of cracks continued to expand with the right tunnel continuous excavation and the beginning of left tunnel excavation. To study the causes and distribution characteristics of cracks, the field investigation and statistics of secondary lining concrete cracks were carried out. Figure 8 presented the statistics of secondary lining concrete cracks of YK39 + 866-YK39 + 910 in right tunnel.

There were two main types of cracks in secondary lining concrete: longitudinal cracks and circumferential cracks, of which longitudinal cracks were the main ones, accounting for more than three quarters. The cracks were mainly concentrated at vault, arch shoulder and arch waist, accounting for 86.21% of the total crack number, and the cumulative length also accounts for 83.5% of the total crack length. A lot of cracks appeared at vault, including the longitudinal cracks and circumferential cracks. The cracks appearing at the arch shoulders and arch waists were all longitudinal cracks. Although the number of cracks at two sides was little different, the right concrete cracking was more serious than that on the left. Especially in YK39 + 882-YK39 + 900, a longitudinal crack with a length of 18.2 m and a maximum width of 4.2 mm appeared at right arch waist (Fig. 8). The maximum crack depth was 245 mm, which was close to half the thickness of the lining. This crack tended to extend and develop in the excavation direction with tunnel construction. The number and scale of cracks at left arch shoulder and waist were relatively small, and no cracks appeared after YK39 + 896. Compared with the right tunnel, there were only

two obvious longitudinal cracks in the lining concrete at left tunnel portal. One was located at vault, with a length of about 9.0 m and a maximum width of 0.45 mm; another was located at right arch waist, with a length of about 6.9 m and a maximum width of 0.38 mm.

4 Analysis Of Failure Mechanism Of Supporting Structures

During the construction process of tunnel portal, distresses such as the failure of slope, the block falling of primary support concrete, the cracking of invert and secondary lining concrete occurred frequently. These distresses posed a serious danger to the tunnel structure safety, and buried potential safety hazards for the subsequent tunnel construction and operation. Previous research results indicated that the failure mechanism of tunnel supporting structures were complex and diverse, which were affected by many factors. In this study, the failure mechanism of supporting structures at tunnel portal was analyzed by means of field investigation, deformation monitoring and numerical simulation, so as to provide the theoretical basis for the subsequent treatment measures.

4.1 Field investigation and monitoring

After a large amount of cracks appeared in secondary lining concrete, the construction unit immediately stopped the excavation and organized multiple experts to conduct a detailed investigation on the failure causes of tunnel portal supporting structures. Combined with the laboratory tests, field deformation monitoring and the statistics of lining concrete cracks, it could be found that the broken and loose gravel soil in the shallow buried and severe bias on the terrain are the one of the main reasons for the supporting structures failure. The field monitoring results showed that there was significant uneven deformation at right tunnel portal during the excavation. Figure 5 presented the deformation of typical positions at tunnel portal only after the right tunnel excavation (the white arrow). The monitoring point at vault was moved up by 6 mm, and the left arch waist was sunk by 16 mm, and the right arch waist was shifted 6 mm to the right. After the tunnel portal was excavated, the gravel soil at deep buried side produced a relatively large loose load on tunnel left side, causing the tendency of whole tunnel structure to shift from the upper left to lower right, which led to obvious settlement at left arch waist while the upward movement at vault. As the tunnel right side was shallowly buried, the load generated by the gravel soil was small, and the back pressure generated by the retaining wall was insufficient, which caused the right translation at right arch waist, and the retaining wall cracked when limiting the tunnel structure deformation. According to the statistical results (Fig. 8), the concrete cracking of the left arch was mainly concentrated from portal section to YK39 + 896, and then the cracking was less likely to occur. It indicated that as the excavation progresses, the buried depth above left arch gradually increased, and the bearing arch had gradually formed in surrounding rock. On the contrary, the right arch concrete was less cracked at tunnel portal, but the cracks gradually appeared frequently after YK39 + 875. The surrounding rock at shallow buried side was not deep enough to form the bearing arch, and the loose load acted directly on the supporting concrete. The supporting structures of tunnel at the same section underwent severe bias load, resulting in obvious asymmetrical deformation on the structures, which could prone to crack and spall of the concrete.

The arrival of rainy season and the infiltration of surface water was another main trigger for the support failure at tunnel portal. Soon after the tunnel portal excavation, the rainy season came, and several heavy rainstorms were experienced during the tunnel construction. The water level of the river rose and overflowed, and the surface water collected in the gravel soil layer. The surface and slope cracks caused by the tunnel portal excavation provided the channels for the infiltration of surface water. In the excavation process of right tunnel portal, some construction personnel successively reported that water leakage and dripping occurred in many positions of the supporting concrete. Due to the untimely treatment of the cracks at slope and surface, atmospheric precipitation and surface water infiltrated through the cracks, resulting in the gradual saturation of gravel soil. The physical and mechanical properties of gravel soil deteriorated rapidly after saturation, causing a significant increase in the loose load of surrounding rock acting on the tunnel structure. As a result, the supporting structures at portal were subjected to more serious bias load, and the asymmetrical deformation increased, which ultimately led to the failure and destruction of the slope and supporting structures (Yang et al. 2020; Chen et al. 2020; Zhang et al. 2022; Xie et al. 2021; Duan et al. 2021; Huang et al. 2022).

Another trigger for support failure was that the excavation faces of two tunnels were staggered too close. The minimum distance between the left and right tunnel axis at portal section was only 13.2 m (i. e. 1.2 times the tunnel width), which was a typical small clear-distance tunnel. In the actual construction process at tunnel portal, the influence of the small clear-distance was not fully considered. When the right tunnel was excavated to 8 m, the left tunnel portal began to construction. The supporting measure for interlaid rock was only the 5 m long hollow grouting anchor bolts (Fig. 4). Soon after the left tunnel portal was excavated, the cracks appeared in the slope, retaining wall and primary support concrete in right tunnel. It indicated that the following tunnel excavation had a significant negative impact on the structural stability of prior tunnel, and intensified the failure of the supporting structures in prior tunnel.

4.2 Numerical simulation

To further reveal the failure mechanism of the supporting structures at tunnel portal, the finite difference software FLAC3D 5.0 was used to simulate and analyze the dynamic tunnel portal excavation process.

4.2.1 Model establishment and boundary conditions

A three-dimensional numerical model was established according to the geological exploration data and the slope topography conditions of tunnel portal, as shown in Fig. 9. To eliminate the boundary effect, the distance between model boundaries and tunnel boundaries was three times the tunnel width, and the length of entire model was 100 m. The distance between lower model boundary and tunnel arch bottom was three times the tunnel height, and the upper model boundary was taken to the ground surface. According to the field investigation, the failure of supporting structures mainly occurred in YK39 + 866-YK39 + 910, so the longitudinal length of model was 60 m. In the process of numerical simulation, the normal displacement of four vertical boundaries was constrained, and the displacement in all directions of bottom boundary was constrained, and the top was a free boundary. The established numerical model included 296005 elements and 167004 nodes in total.

In the numerical simulation, the construction process and support parameters at tunnel portal were consistent with the actual situation. That is, the pipe shed was installed before the tunnel excavation, and the retaining wall was constructed on the right side of right tunnel (Fig. 9). The upper and lower bench method was adopted to excavate the right tunnel first, and the construction step length of each cycle was 1.0 m. The primary support was applied immediately after the tunnel portal excavation, while the application of secondary lining was 12 m behind the tunnel face. The excavation of the left tunnel was 8 m behind the right tunnel face.

4.2.2 Material parameters and simulation cases

In this simulation, the failure of surrounding rock followed Mohr-Coulomb yield criterion. Elastic element was used for retaining wall and concrete. The specific simulation parameters were shown in Table 1. The cable element was used to simulate the pre-grouting pipes and anchor bolts. The grouting reinforcement effect was achieved by increasing the strength of surrounding rock in the reinforcement area. The beam element was used to simulate the pipe shed. The specific simulation parameters of the pipes, anchor bolts and pipe shed were shown in Table 1–2.

Table 1
Parameters of surrounding rock, retaining wall and supporting structures

Material types	Unit weight (kN/m^3)	Elastic modulus (MPa)	Poisson's ratio	Cohesion (kPa)	Internal friction angle (°)
Gravel soil	18.5	50	0.42	20	18.6
Saturated gravel soil	21.6	32.5	0.45	12.6	13.2
Slate with sandstone	20.4	1560	0.24	110	39.2
Retaining wall	25.0	28000	0.2		
Primary support	25.0	28000	0.2		
Secondary lining	25.0	31000	0.2		
Advanced small pipe	78.5	210000	0.3		
Anchor bolt	78.5	210000	0.3		

Table 2
Parameters of pipe shed

Length (m)	Elastic modulus (GPa)	Poisson's ratio	Cross-sectional area (m^2)	Polar moment of inertia (m^4)	Secondary moment of Y axis (m^4)	Secondary moment of Z axis (m^4)
40	65.6	0.262	1.88×10^{-3}	9.82×10^{-6}	4.91×10^{-6}	4.91×10^{-6}

According to the field investigation results, the rainy season came soon after the tunnel portal excavation. Atmospheric precipitation and surface water infiltrated through the cracks into the surrounding rock. Therefore, the influence of water infiltration was also taken into account in the simulation. Based on the model in Fig. 9, three excavation cases were simulated: ① only right tunnel was excavated; ② the right tunnel was excavated first, and the left tunnel was excavated 8 m behind the right tunnel face; ③ on the basis of case 2, considering the influence of surface water infiltration, the saturated gravel soil parameters were used to replace the original surrounding rock parameters. The parameters of saturated gravel soil were obtained from laboratory triaxial test, as shown in Table 1.

4.2.3 Analysis of simulation results

Two typical sections of YK39 + 871 and YK39 + 902 at right tunnel were selected to analyze the deformation and stress characteristics of surrounding rock and supporting structures.

Figure 10 presented the deformation of surrounding rock and supporting structures at YK39 + 871 under three cases. Table 3 showed the field monitoring results and numerical simulation results of surrounding rock deformation at various positions at this section under case ②, in which the vertical deformation was positive upward and the horizontal deformation was positive to the right. Combined with Fig. 10 (a) and Table 3, after the right tunnel portal excavation, the deformation of surrounding rock and supporting structures presented obvious asymmetry due to the influence of topographic bias. The maximum deformation occurred at left arch shoulder, reaching 25.181 mm. As the tunnel left side was deep buried side, the tunnel structure was shifted to lower right under the significant loose load generated by the gravel soil at left side. These deformation characteristics were consistent with the field monitoring results. The deformation of retaining wall showed the characteristics of rotating clockwise with wall corner as the center, that is, the deformation value gradually increased from wall corner to wall top. Form Table 3, it could be seen that the simulation results of surrounding rock deformation at various positions in YK39 + 871 section were in good agreement with the monitoring results. It indicated that the established numerical model and the simulation parameters were conformed to the actual project, and the calculation results were reasonable and feasible.

Table 3
Comparison between field monitoring and numerical simulation of deformation at YK39 + 871 section (unit: mm)

Positions		Field monitoring value	Numerical simulation value
Vault	Vertical deformation	6.0	4.78
	Horizontal deformation	9.0	9.75
Left arch waist	Vertical deformation	-16.0	-15.36
	Horizontal deformation	18.5	19.23
Right arch waist	Vertical deformation	1.5	1.27
	Horizontal deformation	6.0	6.42

From the Fig. 10 (a)-(b), the left tunnel excavation had an obvious negative influence on the stability of right tunnel. After the left tunnel portal excavation, the surrounding rock deformation at right tunnel increased significant, and the asymmetrical deformation and tendency of right tunnel to shift to right was more pronounced. The deformation at the left arch shoulder increased from 25.181 mm to 36.663 mm. It showed that under small clear-distance tunnel arrangement, the following tunnel excavation could aggravate the prior tunnel deformation, which was not conducive to the prior tunnel stability. Comparing Fig. 10 (a)-(c), after the gravel soil was immersed and deteriorated, the asymmetrical loose load on tunnel portal increased sharply. The deformation at left arch shoulder surged to 90.878 mm, and the deviation trend of tunnel structure from deep buried side to shallow buried side was further intensified.

Figure 11 presented the deformation of surrounding rock and supporting structures at YK39 + 902 under three cases. Comparing Fig. 10 and Fig. 11, the surrounding rock load borne by tunnel structures gradually increased with the thickness of overlying surrounding rock gradually increased, resulting in the deformation of surrounding rock and supporting structures also gradually increased. The deformation was still asymmetry and the maximum deformation position of surrounding rock was transferred from left arch shoulder to right side of vault (Fig. 11a-b). Comparing Fig. 11 (a) and (b), the following tunnel excavation aggravated the surrounding rock deformation of prior tunnel, and the maximum deformation at vault increased from 58.525 mm to 76.385 mm. After the gravel soil layer was immersed and deteriorated, the surrounding rock deformation at vault surged to 99.296 mm, and the maximum deformation shifted from vault to slope surface. It indicated that the slope instability was prone to occur under case □. Thus, it was recommended to take some auxiliary measures for slope waterproofing and drainage and stabilized the stratum before excavation.

Figure 12 presented the tensile stress of the retaining wall at YK39 + 871, and Fig. 12 (a) was the tensile stress nephogram of the retaining wall under case □. After the tunnel portal were excavated, the right tunnel tended to shift to right under the loose rock load on deep buried side, and the retaining wall built on the shallow buried side could effectively limit the tunnel deviation. However, the significant deformation of tunnel could cause obvious tensile stress on the retaining wall body, especially at points A and B in

Fig. 12 (a). Figure 12 (b) showed the tensile stress at points A and B under various cases. When only right tunnel was excavated, the maximum tensile stress on the retaining wall appeared at point B, reaching 0.358 MPa. After the left tunnel was excavated, the maximum tensile stress was transferred to point A, reaching 1.071 MPa. After the gravel soil was immersed and deteriorated, the tensile stress at point A increased sharply to 2.031 MPa, which had exceeded the ultimate tensile strength of C25 concrete (JTG 3370.1–2018). At the same time, the tensile stress at point B also increased to 1.847 MPa. Comparing Fig. 12 (a) with Fig. 5, the tensile stress concentration position of the retaining wall obtained by numerical simulation was consistent with the cracking position of the retaining wall in actual project. It indicated that the retaining wall body cracked due to excessive tensile stress in the process of limiting the tunnel deviation.

Figure 13–14 presented the tensile stress and shear stress of primary support concrete at two typical sections, respectively. From Fig. 13 (a) and Fig. 14 (a), affected by the loose rock load on the deep buried side, the maximum tensile stress and shear stress at YK39 + 871 appeared between left arch shoulder and waist under case Ⅱ, that is, the position with the maximum deformation of tunnel. After the left tunnel was excavated, the maximum tensile stress increased from 1.703 MPa to 1.952 MPa (Fig. 13c), which was very close to the ultimate tensile strength of C25 concrete (JTG 3370.1–2018). The maximum shear stress also increased from 1.501 MPa to 2.328 MPa (Fig. 14c). The concrete at arch shoulder and waist was prone to cracked due to obvious tensile stress and shear stress. As the excavation progresses, the thickness of overlying soil increased, and the position subjected to the maximum tensile stress and shear stress on the primary support concrete shifted to right shoulder (Fig. 13b and 14b), that is, the position with the maximum deformation of tunnel at YK39 + 902. After the left tunnel excavation, the maximum tensile stress and shear stress increased from 1.387 MPa and 1.042 MPa to 1.826 MPa and 1.728 MPa, respectively (Fig. 13c and 14c). And then the maximum tensile stress and shear stress increased rapidly to 2.555 MPa and 2.881 MPa when the surrounding rock was immersed and deteriorated. Under such significant tensile stress and shear stress, the primary support concrete was easily cracked, peeled and even collapsed. The stress concentration position was also consistent with the position of cracking and falling blocks of the primary support concrete in actual project (Fig. 6).

Figure 15–16 presented the tensile stress and shear stress of secondary lining concrete at two typical sections, respectively. According to the Fig. 15 (a) and 16 (a), the maximum tensile stress and shear stress of secondary lining concrete at YK39 + 871 appeared between left arch shoulder and waist in case Ⅱ, which was consistent with the stress concentration position of primary support concrete. From the Fig. 15 (c) and 16 (c), after the excavation of left tunnel and the water immersion deterioration of surrounding rock, the tensile stress and shear stress increased rapidly, and the tensile stress reached 2.107 MPa in case Ⅱ, which was very close to the ultimate tensile strength of C30 concrete (JTG 3370.1–2018). Therefore, the secondary lining concrete at left arch shoulder and waist was most likely to crack due to excessive tensile stress (Fig. 15a and 16a). It was also consistent with the crack distribution characteristics in actual project, that is, the number of secondary lining cracks at left arch shoulder and waist at tunnel portal was significantly more than that in other positions in Fig. 8 (a). As the excavation progresses, the maximum tensile stress shifted to between vault and right shoulder (Fig. 15b). The

maximum tensile stress increased to 2.292 MPa in case (Fig. 15b-c), which had exceeded the ultimate tensile strength of C30 concrete. The secondary lining concrete at YK39 + 902 had shear stress concentration at right arch shoulder and waist (Fig. 16b). The maximum shear stress could reach 2.48 MPa in case (Fig. 16b-c), and the concrete at these positions was prone to crack due to excessive shear stress. From Fig. 15 (b) and 16 (b), the tensile stress and shear stress concentration positions coincided with the concentrated distribution positions of secondary lining cracks at this section in Fig. 8 (a).

5 Treatment Measures

From the results of field investigation, deformation monitoring and numerical simulation, it could be found that the shallow buried and asymmetrical loading, surface water infiltration and improper construction were the main triggers for the failure of supporting structures at tunnel portal. Combining the failure mechanism and in consideration of the continuous development of cracks in the tunnel, a series of treatment measures that ‘stabilize the stratum first and then treat the cracks’ were proposed.

5.1 Specific treatment measures

5.1.1 Stratum stabilization measures

First, during the tunnel portal excavation, the shallow buried side of right tunnel was backfilled and compacted in time (Fig. 17). The backfilling height was 3.0 m higher than tunnel vault, and the backfilling slope rate was 1:1.5, and compactness was more than 90%. And then the slope rubble was adopted for slope protection.

Secondly, according to the characteristics of small clear-distance tunnel, the stability of interlaid rock was taken as the construction focus during the excavation. The ground surface grouting was carried out for interlaid rock in the tunnel shallow buried section (YK39 + 856-YK39 + 914.5). The grouting pipes were made of φ89 mm×6 mm hot-rolled seamless steel pipes, with a spacing of 75 cm×75 cm and quincunx arrangement. Each pipe penetrated 5.0 m into the bedrock layer, as shown in Fig. 18. The cement slurry with water cement ratio of 1:1 was adopted as grouting slurry, and the grouting pressure was 0.5–1.5 MPa, and the diffusion radius of single hole slurry was more than 100 cm. Due to the high cost of ground surface grouting in non-shallow buried section, the grouting in the tunnel was adopted to strengthen the interlaid rock column. The 5.0 m long R25 hollow grouting bolts were replaced by 6.0 m long φ42 mm×4 mm hot-rolled seamless steel pipes, arranged at 75 cm in longitudinal direction and 100 cm in circumferential direction. The grouting parameters were consistent with ground surface grouting.

5.1.2 Cracks treatment measures

For the distresses of slope cracks and surface cracks, trenches with a depth of 1.0 m and a width of 0.6 m were dug along the direction of cracks, and then the trenches were backfilled and compacted, and finally covered with waterproof geotextile to prevent the surface water infiltration. For the cracking of retaining wall, repaired the retaining wall cracks, and demolished and rebuilt the severely cracked part.

The humus soil and soft soil at the base of retaining wall were removed, and the rubble was used to replace and compacted. Then, four 3.5 m long foot locking bolts were added at each steel arch in tunnel portal, and installed obliquely downward at right arch foot with 30°-45°.

For the large area falling of primary support concrete at YK39 + 902-YK39 + 910, the construction spacing of steel arches was shortened from 75 cm to 50 cm. And the length of small grouting pipes was increased from 3.0 m to 5.0 m. For the invert cracks at portal, the concrete within 75 cm on both sides of the cracks were removed to the depth of invert bottom, and then grouted with cement slurry. Then, the C25 concrete was used to fill to the top surface of the backfill layer.

According to the cracking degree of secondary lining, different treatment measures were adopted to repair it: For cracks with a depth of less than 5 cm, the low-pressure rapid grouting method was used to fill the cracks. That is, a U-shaped groove with a width of 2 cm and a depth of 1 cm was cut out at crack, and then wiped the groove surface with acetone and filled the groove with epoxy resin mortar, and finally painted the crack surface with epoxy resign slurry. For cracks with a depth of more than 5 cm but less than 15 cm, grooves with a width of 50 cm were cut out on the both sides of cracks with same depth as the crack depth, and then C30 concrete was used for backfilling and pouring. For the cracks with a depth of more than 15 cm, the secondary lining at cracked section was demolished and reconstructed (Fig. 19), and adjusted the φ22 circumferential steel bars to φ28 in lining.

5.1.3 Other auxiliary measures

To reduce the impact of precipitation and surface water infiltration, the intercepting ditches were constructed at the slope top of tunnel portal. To reduce the negative impact of the following tunnel excavation on the structural stability of prior tunnel, the excavation was carried out in strict accordance with the principle that the following tunnel face must be at least 20 m behind the prior tunnel lining section. During the portal excavation, the principle of short excavation and short advance should be followed, and the invert needed to closed into a ring in time. Finally, the cracks observation was taken as the focus of monitoring, and gave feedback of the cracks development timely. Combined with other monitoring data, fully grasped the treatment effect, so as to dynamically adjust the treatment measures.

5.2 Evaluation of treatment measures

To better grasp and evaluate the treatment measures effect, steel string concrete strain gauges were arranged in the secondary lining concrete at YK39 + 890 (lining demolition and reconstruction section) and YK39 + 930 (subsequent excavation section). The lining concrete stress at vault, arch shoulder, arch waist and arch foot was monitored and analyzed. The buried positions and monitoring results were shown in Fig. 20. After the implementation of treatment measures, the stress distribution at secondary lining concrete was still asymmetric, and the concrete stress at shallow buried side was more unfavorable than that at deep buried side (Fig. 20b-c). The maximum tensile stress still occurred at right arch shoulder, reaching 1.089 MPa and 0.482 MPa, but the value had not yet reached the ultimate tensile strength of C30 concrete, which had a certain safety reserve. It indicated that the secondary lining stress had been significantly ameliorated. Moreover, the uneven stress of lining concrete had been alleviated to a certain

extent with the construction of auxiliary measures and the increase of buried depth, and the concrete at vault and left shoulder no longer underwent the tensile stress, which meant that the surrounding rock quality was strengthened effectively and the bearing arch had gradually formed.

After the stratum stabilization measures were completed, the field monitoring results of surrounding rock tend to be stable, and the maximum settlement value did not exceed 30 mm. There was no more obvious cracking or water seepage in the concrete after the cracks were repaired. Overall, the proposed and implemented treatment measures had achieved the expected results.

6 Conclusions

In this paper, a shallow buried and asymmetrically loaded tunnel with small clear-distance in northwest China was taken as an engineering case. In response to the distresses occurred at tunnel portal such as instability of the slope, spalling of the primary support, and cracking of the secondary lining, in-depth research on the failure mechanism of support structures was carried out combining with field investigation, statistical analysis, monitoring measurement and numerical simulation. Then, a series of treatment measures were proposed and the effect were evaluated. The following conclusions can be drawn from this study:

(1) The topography at tunnel portal was shallow buried and asymmetrically loaded, and the gravel soil layer was broken, loose and unstable. The construction coincided with rainy season, surface water seeped into the surrounding rock along the slope and surface cracks, further deteriorating the physical and mechanical properties of the surrounding rock. After tunnel portal excavation, the supporting structures underwent significant asymmetrical loose load, resulting in cracking and failure due to excessive local deformation. In addition, the staggered distance between the left and right tunnels during the excavation process was too short, and the interlaid rock was not reinforced effectively. As a result, the excavation of following tunnel had an obvious negative impact on the stability of prior tunnel, and aggravated the failure of the supporting structure at prior tunnel.

(2) The field monitoring and simulation results indicated that after tunnel portal excavation, the loose load generated by the surrounding rock at deep buried side could cause the entire tunnel to deviate to shallow buried side. In the process of limiting tunnel deformation, the retaining wall produced a clockwise rotation deformation around the wall corner, and partial wall cracked due to obvious tensile stress. After the surrounding rock was immersed and deteriorated, serious asymmetrical deformation and stress concentration occurred at the primary support and secondary lining due to the obvious asymmetrical loose load, resulting in the cracking and failure of concrete.

(3) Combining with the failure mechanism of supporting structures and the characteristics of continuous development of cracks, a series of treatment measures that ‘stabilize the stratum first and then treat the cracks’ were proposed. The specific measures included backfilling and compacting the shallow buried side of tunnel portal, reinforcing the interlaid rock by ground surface grouting, constructing the intercepting ditches at the slope top, and excavating the following tunnel 20 m behind the lining section

of prior tunnel. The results of field inspection and stress monitoring indicated that after the treatment measures were implemented, the supporting concrete stress was ameliorated effectively. There was no obvious cracking or water leakage during the subsequent tunnel construction, indicating that the proposed measures had achieved good treatment effect.

Declarations

Conflict of Interest

The authors declare that there is no conflict of interest in the manuscript.

Acknowledgments

The authors acknowledge the financial support provided by the National Natural Science Foundation of China (Grant No. 51978064), Natural Science Foundation of Shanxi Province (Grant No. 2018JQ5001), Natural Science Foundation of Shaanxi Province (Grant No. 2021JQ-253), Hubei Key Laboratory of Roadway Bridge and Structure Engineering (Wuhan University of Technology, No. DQJJ202104) and by the Fundamental Research Funds for the Central Universities, CHD (Grant Nos. 310821163302, 300102210213, 300102210304).

References

1. Bai Z, Wu SC (2012) Calculation method of surrounding rock pressure for shallow and unsymmetrical tunnel under deep valley terrain. Appl Mech Mater 170–173:1382–1387
2. Chen H, Lai HP, Qiu YL, Chen R (2020) Reinforcing distressed lining structure of highway tunnel with bonded steel plates: case study. J Perform Constr Facil 34(1):04019082
3. Cui SS, Wu K, Zhang QJ, Yu YL, Wang YJ (2019) Analysis on construction mechanical mechanism of highway tunnels with large span and small spacing. Geotech Geol Eng 37:1627–1642
4. Duan X, Hou TS, Jiang XD (2021) Study on stability of exit slope of Chenjiapo tunnel under extreme rainstorm conditions. Nat Hazards 107(2):1387–1411
5. Huang XH, Wang L, Ye RQ, Huang HF, Guo F, Huang GL (2022) Study on deformation characteristics and mechanism of reactivated ancient landslides induced by engineering excavation and rainfall in Three Gorges Reservoir area. Nat Hazards 110(3):1621–1647
6. Jiang K, Xia CC, Bian YW (2012) Optimal analysis of construction schemes of small space tunnel with bidirectional eight traffic lanes in jointed rock mass. Rock Soil Mech 33(2):841–847 (in Chinese)
7. Jiang Q, Song SG, Li T, Wang K, Gu RH (2019) Study on surrounding rock stability of small clear-distance twin highway tunnel with eight lanes. Geotech Geol Eng 37:593–598
8. Jiao P, Ma L, Wu YZ (2019) L Y Study on effect of late tunnels on deformation of early tunnel in three small net distance tunnels. IOP Conference Series: Earth and Environmental Science 267:42099

9. Kawada T, Otsuka M, Kobayashi M (1996) Observation and construction of large two-lane highway tunnel with minimum spacing. Hydropower Technol Inform Z01:146–154
10. Kim SH (2004) Interaction behaviours between parallel tunnels in soft ground. Tunn Undergr Space Technol 19:448
11. Lee CJ, Jacobsz SW (2006) The influence of tunnelling on adjacent piled foundations. Tunn Undergr Space Technol 21:3–4
12. Lei MF, Peng LM, Shi CH (2015) Model test to investigate the failure mechanisms and lining stress characteristics of shallow buried tunnels under unsymmetrical loading. Tunn Undergr Space Technol 46:64–75
13. Liu XR, Chen HJ, Liu K, He CM (2017) Model test and stress distribution law of unsymmetrical loading tunnel in bedding rock mass. Arab J Geosci 10(7):184
14. Lv JB, Li XL, Li ZR, Fu HL (2020) Numerical simulations of construction of shield tunnel with small clearance to adjacent tunnel without and with isolation pile reinforcement. KSCE J Civ Eng 24(1):295–309
15. Pan HK, Zhang YG, Hu JC, Yang LD (2011) The mechanics analysis and feedback design for shallow multi-arch tunnel under unsymmetrical pressure. Adv Mater Res 261–263:1114–1118
16. Qiu YJ, Peng LM, Lei MF (2015) Upper bound solutions for surrounding rock pressure of shallow bias tunnel. China Civil Eng J 48(6):106–113 (in Chinese)
17. The Professional Standards Compilation Group of People's Republic of China (2019) Code for Design of Road Tunnel (JTG 3370.1–2018). China Communications Press, Beijing. (in Chinese)
18. Wen D, Poh J, Ng YW (2004) Design considerations for bored tunnels at close proximity. Tunn Undergr Space Technol 19(4–5):22–27
19. Xia CC, Gong JW, Tang Y, Zhu HH (2007) Study on site monitoring of large-section highway tunnels with small clear spacing. Chin J Rock Mech Eng 26(1):44–50 (in Chinese)
20. Xiao JZ, Dai FC, Wei YQ, Min H, Chong X, Tu XB, Wang ML (2014) Cracking mechanism of secondary lining for a shallow and asymmetrically-loaded tunnel in loose deposits. Tunn Undergr Space Technol 43:232–240
21. Xiao JZ, Dai FC, Wei YQ, Xing YC, Cai H, Xu C (2016) Comparative analysis of excavation schemes for a tunnel constructed through loose deposits. J Perform Constr Facil 30(4):04015061
22. Xie WL, Guo QY, Wu JY, Li P, Yang H, Zhang MS (2021) Analysis of loess landslide mechanism and numerical simulation stabilization on the Loess Plateau in Central China. Nat Hazards 106(1):805–827
23. Yang C, Hu ZX, Huang D, Guo F (2020) Failure mechanism of primary support for a shallow and asymmetrically loaded tunnel portal and treatment measures. J Perform Constr Facil 34(1):04019105
24. Yang C, Zhang YX, Huang D, Zhu Q (2013a) Deformation behavior of topographic unsymmetrical loaded tunnels and their pre-reinforcements after excavation. J Highway Transp Res Dev (English

Edition) 7(3):69–75

25. Yang XL, Wang JM (2018) Stress dilatancy analysis of shallow tunnels subjected to unsymmetrical pressure. J Cent South Univ 15(S2):28–33
26. Yang XL, Zhang JH, Jin QY, Ma JQ (2013b) Analytical solution to rock pressure acting on three shallow tunnels subjected to unsymmetrical loads. J Cent South Univ 20(2):528–535
27. Zhang B, Wang X, Zhang JS, Zhang JH, Cheng H (2018) Safe range analysis of clear distance of twin shallow tunnels based on limit analysis and reliability theory. J Cent South Univ 25(1):196–207
28. Zhang YX, Shi YF, Zhao YD, Fu LR, Yang JS (2017) Determining the cause of damages in a multiarch tunnel structure through field investigation and numerical analysis. J Perform Constr Facil 31(3):04016104
29. Zhang YX, Yuan MQ, Lu WH, Zhan J (2022) Cause investigation of ground sliding during tunneling in sloping and stratified stratum. Nat Hazards 111(2):1421–1430
30. Zuo CQ, Chen JP, Liu H (2011) Load calculation method of tunnels with shallow buried depth and unsymmetrical pressure in regions of weak fissured surrounding rock. Adv Mater Res 243:3364–3369

Figures

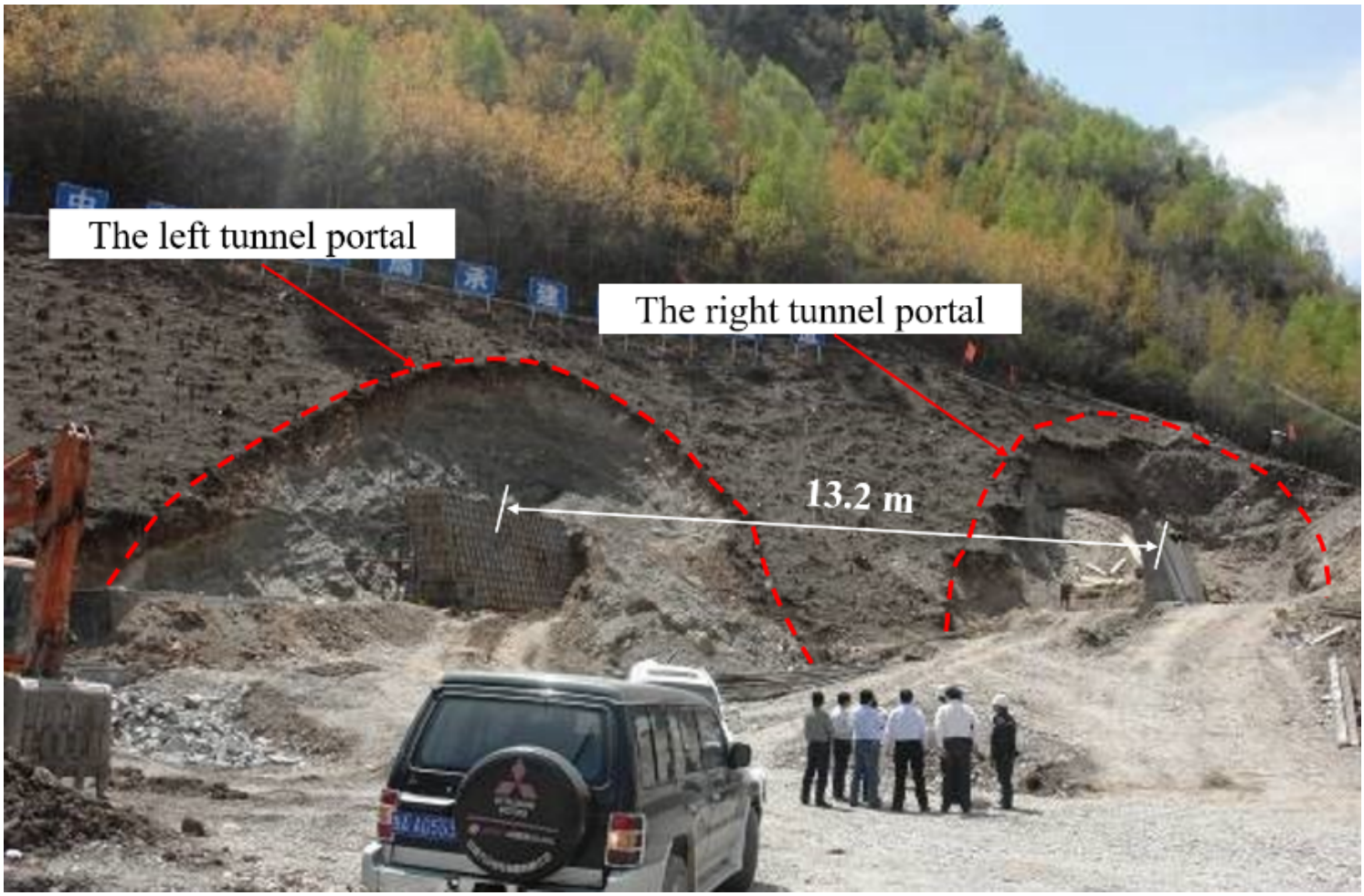

Figure 1

The portal section of tunnel

Figure 2

The portal section of tunnel

Figure 3

The shallow buried and asymmetrically loaded situation at the right tunnel portal

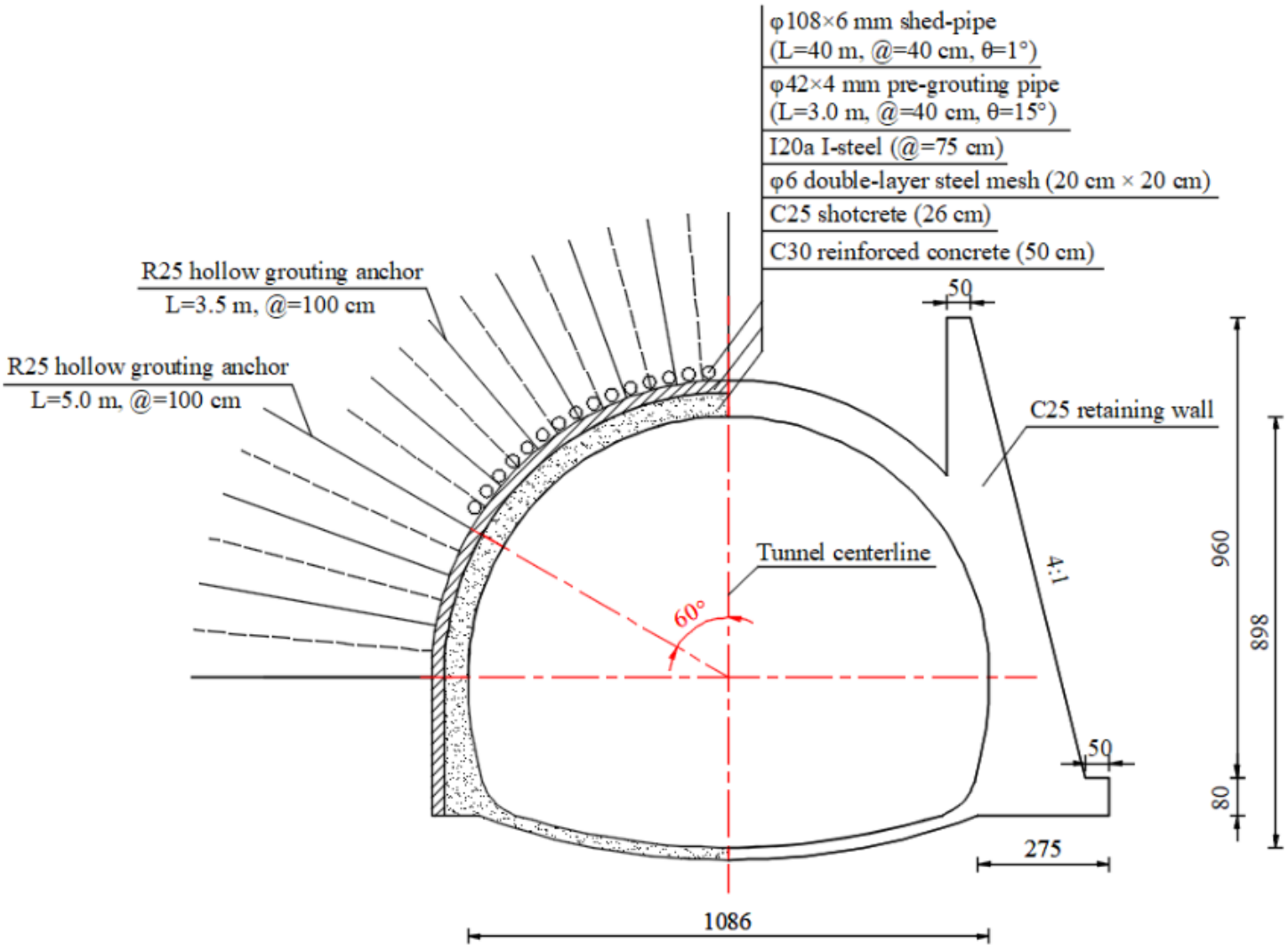

Figure 4

The supporting measures at right tunnel portal

Figure 5

Failure of the right tunnel slope and retaining wall

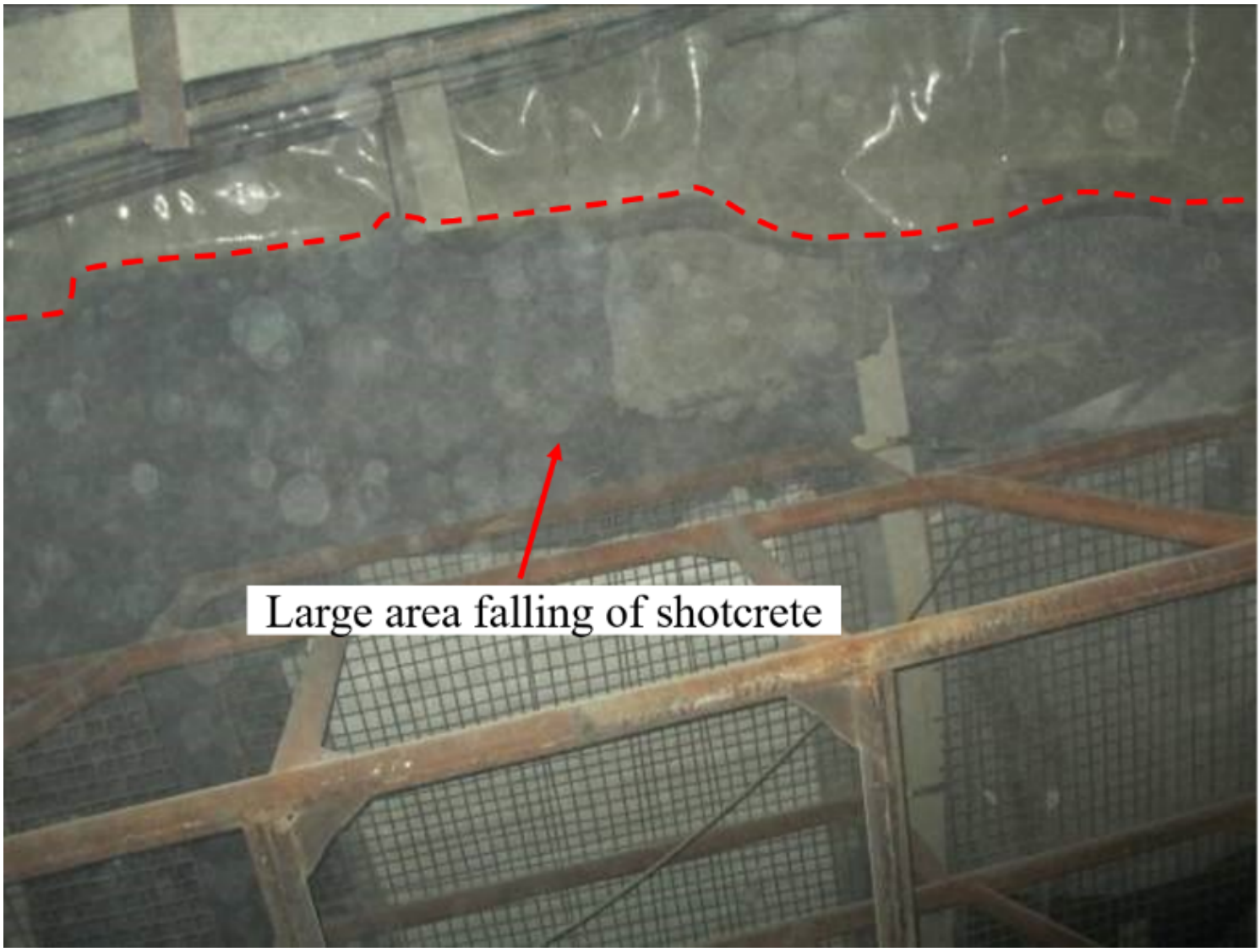

Figure 6

Block falling of the primary support concrete at the right tunnel

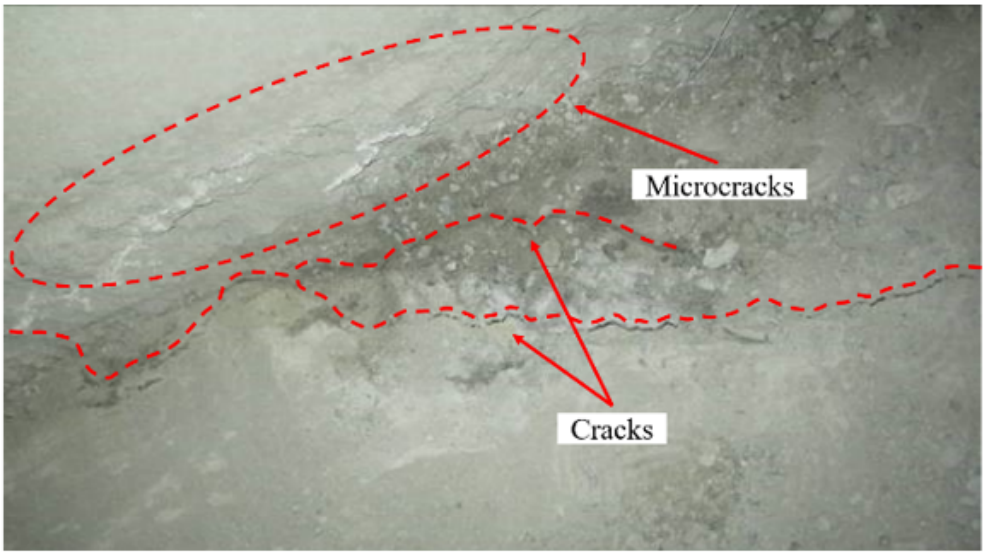

(a) The right tunnel

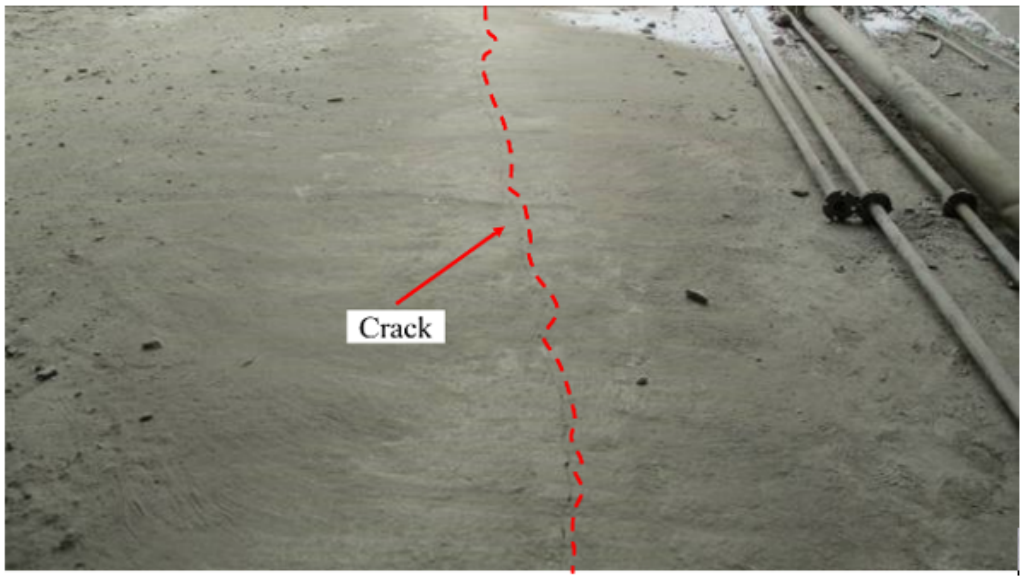

(b) The left tunnel

Figure 7

Cracking of the invert at tunnel portal

Figure 8

Statistics of the cracks in secondary lining concrete at right tunnel

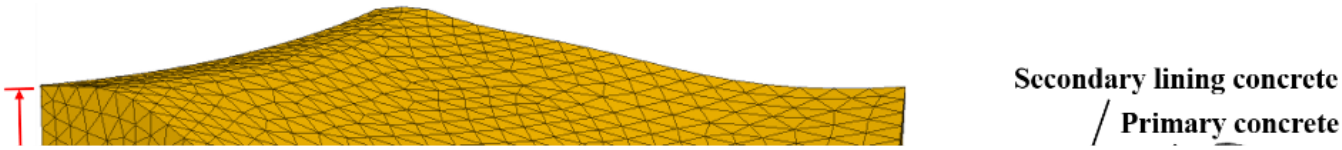

Figure 9

Three-dimensional numerical model

Figure 10

Deformation of surrounding rock and supporting structures at YK39+871 section under various cases (unit: m)

Figure 11

Deformation of surrounding rock and supporting structures at YK39+902 section under various cases (unit: m)

Figure 12

Tensile stress of the retaining wall

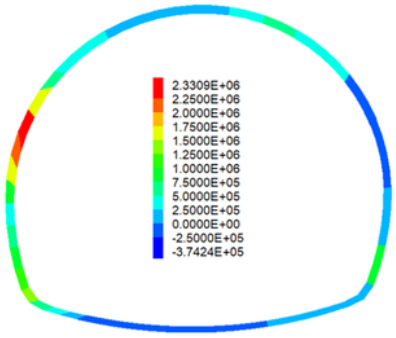

(a) Tensile stress nephogram of the primary support concrete at YK39+871 in case III (unit: MPa).

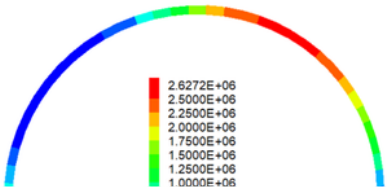

Figure 13

Tensile stress of the primary support concrete

Figure 14

Shear stress of the primary support concrete

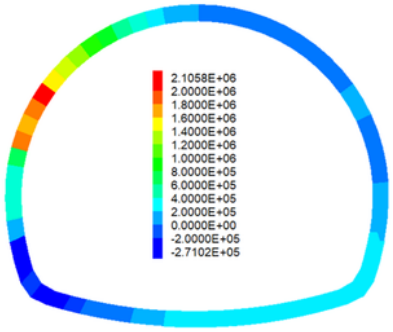

(a) Tensile stress nephogram of the secondary lining concrete at YK39+871 in case III (unit: MPa).

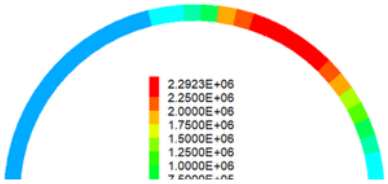

Figure 15

Tensile stress of the secondary lining concrete

Figure 16

Shear stress of the secondary lining concrete

Figure 17

The shallow buried side was backfilled and compacted

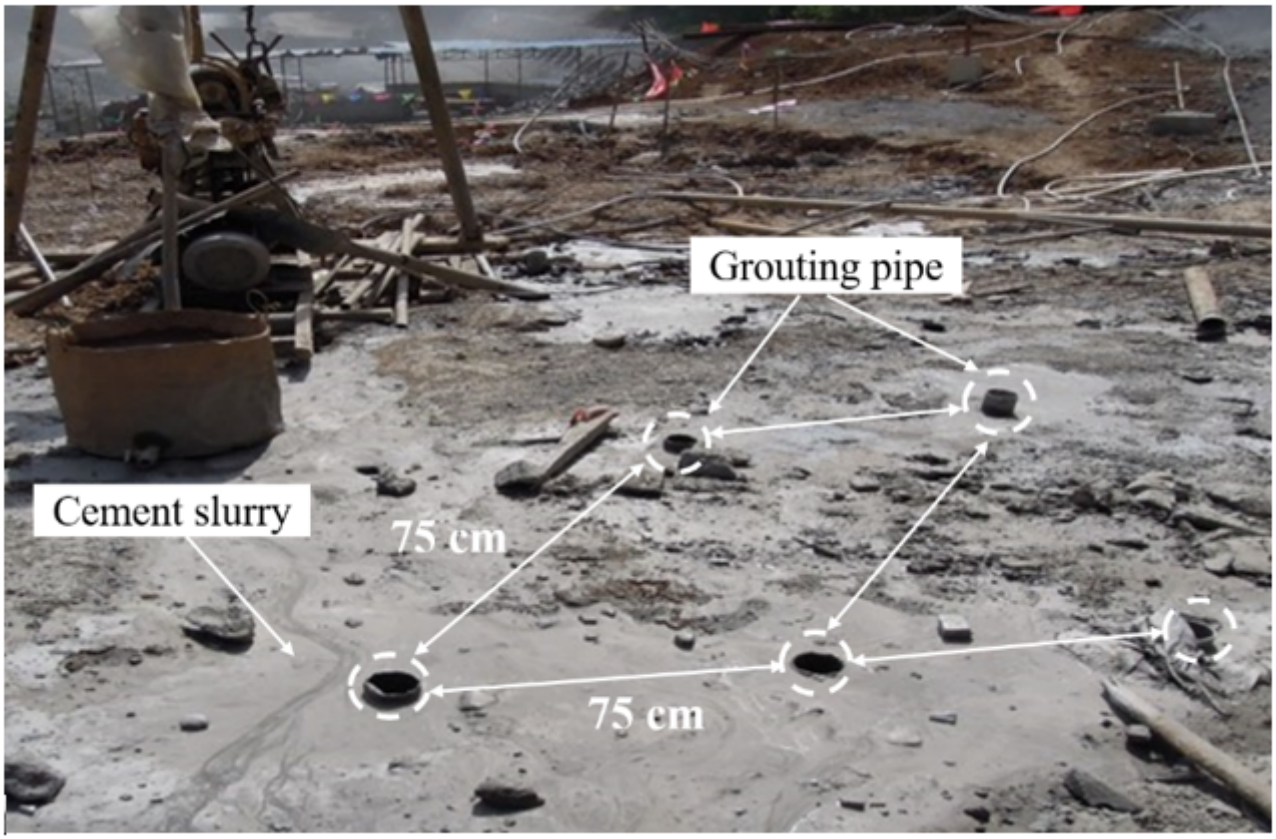

Figure 18

Ground surface grouting reinforcement of the interlaid rock

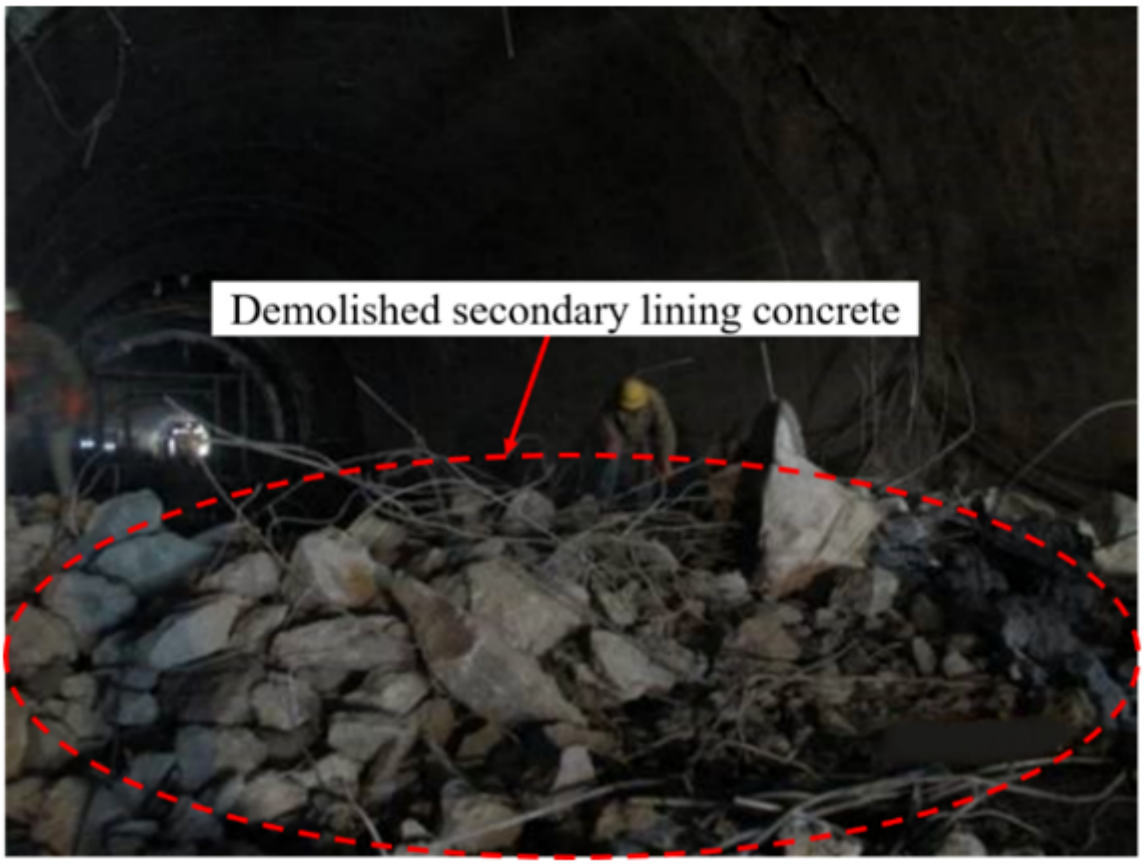

Figure 19

Demolition and reconstruction of the severely cracked secondary lining concrete

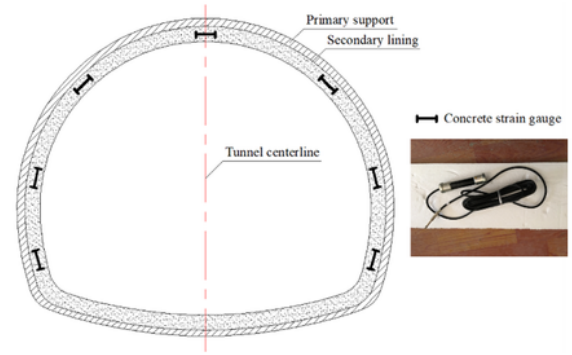

(a) Buried positions of concrete strain gauges.

(b) Stress of secondary lining concrete at YK39+890.

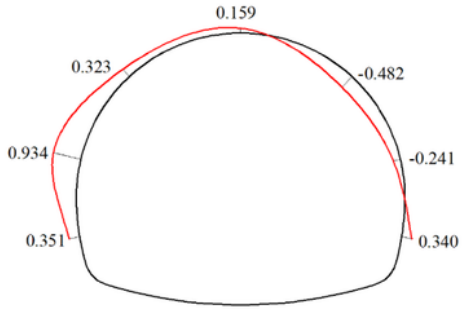

(c) Stress of secondary lining concrete at YK39+930.

Figure 20

Field monitoring of secondary lining concrete stress (unit: MPa, positive value means compressive stress, while negative value means tensile stress)